Summer 8-2021

Effect of Ultrasound Pressure on the Distribution of Bovine Serum Albumin Delivered by Focused Ultrasound-mediated Blood-Brain Barrier Opening in Cleared Mouse Brains

Yajie Liu
Washington University in St. Louis

Washington University in St. Louis

McKelvey School of Engineering

Department of Biomedical Engineering

Thesis Examination Committee:

Hong Chen

Chao Zhou

Song Hu

Effect of Ultrasound Pressure on the Distribution of Bovine Serum Albumin Delivered by

Focused Ultrasound-mediated Blood-Brain Barrier Opening in Cleared Mouse Brains

By

Yajie Liu

A thesis presented to the McKelvey School of Engineering of Washington University in

St. Louis in partial fulfillment of the requirements for the degree of Master of Science

August 2021

St. Louis, Missouri

Acknowledgements

I would like to sincerely thank Prof. Hong Chen for the guidance, encouragement and research resources she provided in the past two years, as well as the opportunity to study and do research in Chen Ultrasound Laboratory, where I met great mentors and friends. I sincerely appreciate Dr. Si Chen for her guidance, patience and help as soon as I met problems. I also want to thank Dr. Dezhuang Ye, Dr. Jinyun Yuan, Yimei Yue, Yan Gong, Chih-Yen Chien, Dr. Zhongtao Hu, Yaoheng Yang, Lu Xu, Kevin Xu, Christopher Pacia, who are friendly members of the lab, for their selfless help. I couldn't have had such a wonderful research experience without them.

I would like to thank Dr. Bayguinov Peter, Dr. Praveen Krishnamoorthy and other staff in Center for Cellular Imaging (WUCCI), for their responsible training, efficient troubleshooting and selflessly sharing their experience on imaging.

I would like to thank Prof. Chao Zhou and Prof. Song Hu for their willingness to be on the committee of my thesis defense.

I appreciate my mother and my father so much for their accompany and support while I was writing my thesis, although there is a very long distance and a 13-hour time difference between my hometown and St. Louis.

Last but not least, I want to thank every women scientist. Their existence and enthusiasm for pursuing the truth always encourage me.

Table of Contents

List of Tables

List of Figures

Abstract

Effect of Ultrasound Pressure on the Distribution of Bovine Serum Albumin Delivered by

Focused Ultrasound-Blood Brain Barrier Opening in Cleared Mouse Brains

By

Yajie Liu

Master of Science in Biomedical Engineering

Washington University in St. Louis, 2021

Research Advisor: Professor Hong Chen

Most common diagnosis and therapeutic methods have low effectiveness when used on brain diseases. The key obstacle is that the blood-brain barrier (BBB) prevents most drugs from entering the brain. Some strategies have been developed to improve the efficiency of drug delivery crossing BBB. Among all these strategies, focused ultrasound-mediated BBB opening (FUS-BBB Opening) stands out since it is noninvasive and can be located to the target area. Detailed studies are required on the distribution of drugs delivered by FUS-BBB opening and the effects of FUS parameters on the distribution. This thesis proposes a pipeline involving tissue clearing and lightsheet microscopy to study the distribution of BSA relative to vessels in mouse brains treated with FUS and the effect of ultrasound pressure on the delivery pattern.

As mentioned before, slices (1 mm thick) from mouse brains treated with FUS were cleared until their transparency meets the requirement of large-volume three-dimensional (3D) imaging. Blood vessels and BSA clusters in the 3D images obtained from lightsheet microscopy were segmented and the distance of every cluster from the nearest vessel was collected in the distance map.

Comparing the distance maps of different pressures, it is indicated that FUS with the pressure of 0.4 MPa significantly increases the amount of BSA clusters in brains, especially those distributed closer to the outer surface of vessels. BSA delivered by 0.2 MPa FUS and 0.4 MPa FUS has different distribution patterns relative to vessels. At the same time, this thesis discussed the feasibility of this pipeline to study FUS-BBB opening-induced drug delivery.

Chapter 1: Introduction

Background

The brain is one of the most important organs of humans. Brain diseases, like central nervous system (CNS) diseases and brain cancers, are troubling many patients. In consequence, research about the physiological mechanism of the brain and the treatment of brain diseases has always attracted attention. However, due to the existence of the blood-brain barrier (BBB), drugs for brain diseases only have poor effects.(Dong, 2018) The advantages of FUS-BBB opening as noninvasive and localized have been validated for the delivery of therapeutic and imaging agents. The distribution of drugs is important to a drug delivery method since it not only plays a key role in clinical safety and efficiency but also helps us to understand the physiological process during the delivery. Pressure amplitude is a main parameter of FUS and has been proved to affect drug delivery crossing BBB. However, studies on the 3D distribution of drugs relative to neuron vascular under different pressures remain blank.

Tissue clearing has been used to visualize the biodistribution of delivered materials in brain tissue as a pre-imaging processing technique because of its advantage in the visualization of intact tissue. Tissue clearing matches the refractive indices of different tissue layers and improves the transmission of light so that it can increase the imaging depth by removal of the light scattering and adsorbing substance.(Arms et al., 2020) On the other hand, it can still provide us with spatial information since it preserves the main structure constituted by proteins. Validated methods can make large samples transparent enough so that the imaging extent is only limited by the working distance of objective lenses. The appearance of tissue clearing techniques helps us to

achieve subcellular 3D imaging without deleterious sectioning on tissue and sophisticated data reconstruction so that we avoid mechanical distortion as much as possible.

Drug Delivery Induced by FUS-BBB Opening

For a long time, how to cross (BBB) has always been the main obstacle to applying many diagnosis and therapeutic methods to brain diseases. Anatomically speaking, BBB is a continuous layer of endothelial cells (ECs) on cerebral vascular. These ECs bound to each other with tight junctions (TJs) and have extremely low rates of transcytosis compared with peripheral ECs, so that restricts the paracellular flux and vesicle-mediated transcellular movement of solutes.(Banks, 2008) ECs and their unique property to limit substance exchange between the vascular system and central nervous system (CNS) together constitute the physiological BBB. In the healthy brain, BBB is important to maintain the homeostasis of the CNS and protect it from toxins and pathogens. However, BBB also prevents most therapeutic materials and imaging agents circulating in the vasculature from arriving at the brain parenchyma, which reduces the efficiency of drug delivery and correspondingly increases the systematic toxicity. Some strategies have been developed to circumvent the BBB. However, intra-cerebral injection, use of implants or convection-enhanced delivery are invasive and raise significant safety concerns. Modifying drugs to take advantage the native BBB transport or transcytosis system requires excessive costs of designing new drugs.(Gabathuler, 2010) Other strategies involving viral vectors, non-viral nanoparticles and brain permeability enhancers have been indicated in recent publications that they may not have enough therapeutic effects at a reasonable dosage of drugs.(Dong, 2018)

Focused ultrasound (FUS) combined with microbubbles (MBs) are discovered to be able to disrupt the integrity of BBB without apparent neuronal injury. Compared with other strategies, FUS-BBB opening is noninvasive and can be localized to the target area. As the research

developed, the successful delivery by FUS-BBB opening has been verified for a wide range of therapeutic and imaging drugs, such as radiolabeled nanoclusters, liposomally-encapsulated drugs and antibodies.

MBs are small-sized (1-5 µm) gas-filled vesicles stabilized by phospholipids, proteins or polymers.(Dasgupta et al., 2016) Ultrasound is most well-known for its application on clinical noninvasive real-time imaging. With ultrasound, MBs in the neuronal vascular may contract, expand or burst, which will trigger a series of biophysical effects. The main consequence of these effects will be the transient opening of ECs and the TJs between ECs leading to the increase of microvascular permeability, thus improving the drug delivery across the BBB. In addition, soft- and hardware techniques on focused ultrasound can limit the BBB opening within small areas, improving the targeting of drug delivery and reducing the risk to the whole brain.

The pressure amplitude of FUS is an important parameter to BBB opening. Increasing the pressure amplitude will increase the BBB permeability. With the same frequency, repetition frequency and total exposure time, higher pressure intend to cause the BBB opening at a larger area and the signal enhancement caused by the increase in the average delivery volume of the magnetic resonance imaging (MRI) contrast agent per unit area.(Chopra et al., 2010) The increase in pressure also tends to enlarge the BBB opening size, defined by the size of the largest molecule that can cross the BBB.(Chen & Konofagou, 2014) However, excessive pressure will cause tissue damage such as hemorrhage, necrotic and neuronal injury.(Chopra et al., 2010)

Tissue Clearing

The main principle of tissue clearing is the substitution of water in samples with the solutions that have higher RI, which is closer to the tissue. In this procedure, the key problem is how to prompt the material exchange between in- and outside tissue. Among all developed

methods, some methods rely on chemical solvents and passive diffuse (passive and active CLARITY, SWITCH). Most tissue clearing methods can be divided into two groups based on the characteristic of the solvents they use: organic solvent (EtOH, THF)–based clearing methods (3DISCO, iDISCO) and hydrophilic reagent (urea, D-sorbitol, fructose)–based clearing methods (ScaleS, AbScale, CUBIC, FRUIT, UbasM, SeeDB). Although some organic solvent and amino alcohol already can solubilize lipids, some methods also add detergent (SDS, Triton X-100) into their recipe to improve the ability of lipid removal, therefore increase the transmission of light, such as CLARITY, SWITCH, AbScale and CUBIC. Active CLARITY involves electrophoresis to accelerate the penetration of detergent into tissue. Besides, although all methods require the tissue to be fixed before clearing, the tissue-hydrogel crosslinking with acrylamide in CLARITY provides more opportunity to retain protein and nanoparticles.

All these tissue clearing methods have their advantages as well as shortages. The characteristics of several typical methods are shown below (Table 1)

Table 1

Comparison of Tissue Clearing Methods

Method and reference	Mechanism of clearing	Procedure time	Tissue integrity	Preservation of fluorescence	IHC compatibility	Nanoparticle retention	Tissue validated
3DISCO(THF/TBE)(Ertürk et al., 2012)	Dehydration with THF, RI homogenization with TBE	1 day for the whole mouse brain	0.8-fold shrinkage	Better for CFP, GFP, RFP, mCherry than YFP, TBE degrades fluorescent signal over time -	Yes	polystyrene-based nanoparticles (~500 nm) degrade ~150-fold, insignificant decrease for melamine resin-based (~500 nm) nanoparticles, quantum dots (~20 nm) remain enough signal-to-background ratio(Yang et al., 2019) -	mouse brain, lung, spleen, lymph nodes, mammary glands and tumor tissues, human brain,
ScaleS(Hama et al., 2015)	RI homogenization via molecule flux by sorbitol and urea	4 days for the whole mouse brain	No significant size changes	Good.	No	Polymeric nanoparticles(Ishizawa et al., 2020)	Mouse brain and human brain, mouse liver
AbScale(Hama et al., 2015)(Hama et al., 2011)	Lipid removal by detergent, RI homogenization by	4 days for 1mm thick mouse brain slice	Undergoes expansion during clearing, shrinks	Good for mCherry, limited for EGFP, GFP-like proteins.	Yes	Unknown	Mouse brain

	glycerol, molecule flux by sorbitol and urea		back after RI homogenization	Signal undergoes some quenching			
CLARITY (active)(Flynn et al., 2015)	Tissue-hydrogel crosslinking with PFA and acrylamide, Lipid removal with SDS, RI homogenization with glycerol, molecule flux by electrophoresis	~6 days for whole mouse brain	Undergoes expansion during clearing, shrinks back after RI homogenization	Good	Yes	After 4 days. ~70% retention for 6 nm PEGylated quantum dots, ~84% retention for 50 nm Au-PEG	Mouse brain, spinal cord, spleen, pancreas, intestine, kidney, lung, testis, and muscle
CLARITY (passive)(Sindhwani et al., 2017)	Tissue-hydrogel crosslinking with PFA and acrylamide, Lipid removal with SDS, RI homogenization with glycerol	~21days for the whole mouse brain	Undergoes expansion during clearing, shrinks back after RI homogenization	Good	Yes	PEGylated quantum dots undergo 12% loss after 6 days	Rodent brain, spinal cord, intestine, kidney, lung, liver, and pancreas; human brain; and zebrafish
SeeDB	RI homogenization via	4 days for the whole mouse brain	No significant size	Good for many types of fluorescent	Yes	unknown	Mouse brain, olfactory bulb.

	molecule flux with aqueous fructose solutions		change and morphological deformations during the whole procedure	dyes, including fluorescent proteins and lipophilic neuronal tracers			
CUBIC(Susaki et al., 2014)	Decolorize the blood via eluting heme by amino alcohol(Tainaka et al., 2014), lipids removal by amino alcohol and detergent, RI homogenization with glycerol and DMSO, molecule influx by urea	10~14 days for the whole brain	Undergoes ~1.35-fold expansion during clearing, shrinks back after RI homogenization	Good for EGFP, EYFP, mCherry and mKate2	YES	axane-encapsulated polymeric nanoparticles remained enough signal-to-background ratio in mouse lung(Cuccarese et al., 2017)	Whole organ of the mouse, tumor

Considering this study can be extended to observe the colocalization of BSA and neuron cells, the IHC compatibility, fluorescence preservation ability and nanoparticle preservation ability of these methods are mainly cared about. After carefully screening and balancing, we pick AbScale as our protocol. As shown in the table, AbScale is compatible with immunohistochemistry and can preserve most fluorescence by the end of tissue clearing. In the protocol of AbScale, reagent-1 (ScaleS0) can solubilize cholesterol of biological membrane with Methyl-β-cyclodextrin and γ-cyclodextrin and loosen collagen structure with N-acetyl-L-hydroxyproline. After the incubation in ScaleS0, the fixed tissue becomes loose enough to exchange materials with the following reagents. Reagent-2 (ScaleA2) involves high concentration urea to prompt the molecule influx, Triton X-100 to extract lipids. Reagent-3 (ScaleB4) has a 2-fold higher concentration of urea to clear the tissue quickly. Reagent-4 (ScaleS4) contains glycerol and DMSO for high RI (1.439). The molecule influx by urea and osmotically balanced molecule flux by D-sorbitol in ScaleS4 accelerate the penetration of the solution.

So far there is a lack of reference on the loss of nanoparticles after clearing by AbScale. However, bovine serum albumin (BSA) as a kind of protein can be linked to the crosslinking formed by close endogenous proteins in the tissue through amino acids during fixation and post-fixation. This process greatly improves the probability of the retention of delivered BSA after tissue clearing, thus providing our study with more accurate information. In addition, BSA is a competitive carrier of drugs, especially nanoparticle delivery drugs, so that involved in the therapy of many kinds of cancers.(Elzoghby et al., 2012) BSA is serum albumin derived from cows and has 583 amino acid residues. The molecule weight of BSA is 69323 Da. The dimension of a single BSA particle is $140 \times 40 \times 40$ Å. BSA is rich in nature and easy to be purified. It also has the advantages of biodegradability, nontoxicity, safe degradation products after metabolized in vivo

and non-immunogenicity. Last but not least, BSA nanoparticles can be prepared by simple coacervation.(Galisteo-González & Molina-Bolívar, 2014) Therefore, BSA is a good drug model for our study.

Chapter 2: Materials and Methods

Animals

Animal protocols used in this study were reviewed and approved by the Institutional Animal Care and Use Committee in accordance with the National Institutes of Health guidelines for animal research (approval no. 20180186; date of approval: 12 August 2019). Cr. NIH Swiss mice (6–8 weeks, ~25 g body weight, female) were ordered from Charles River Laboratory (Wilmington, MA, USA). The animals were housed in a room maintained at 22 °C and 55% relative humidity, with a 12-h/12-h light/dark cycle and access to standard laboratory chow and water.

Drug Model

Albumin from Bovine Serum conjugated with Alexa Fluor™ 647 (BSA-AF647) was purchased from Thermo Fisher Scientific (Wilmington, DE, USA) and dissolved to 1.3 mg/mL with 1x Phosphate Buffered Saline (PBS) when in use.

FUS-BBB Opening Setup

The FUS-BBB opening treatment was finished with an in-house mini transducer.

Workflow

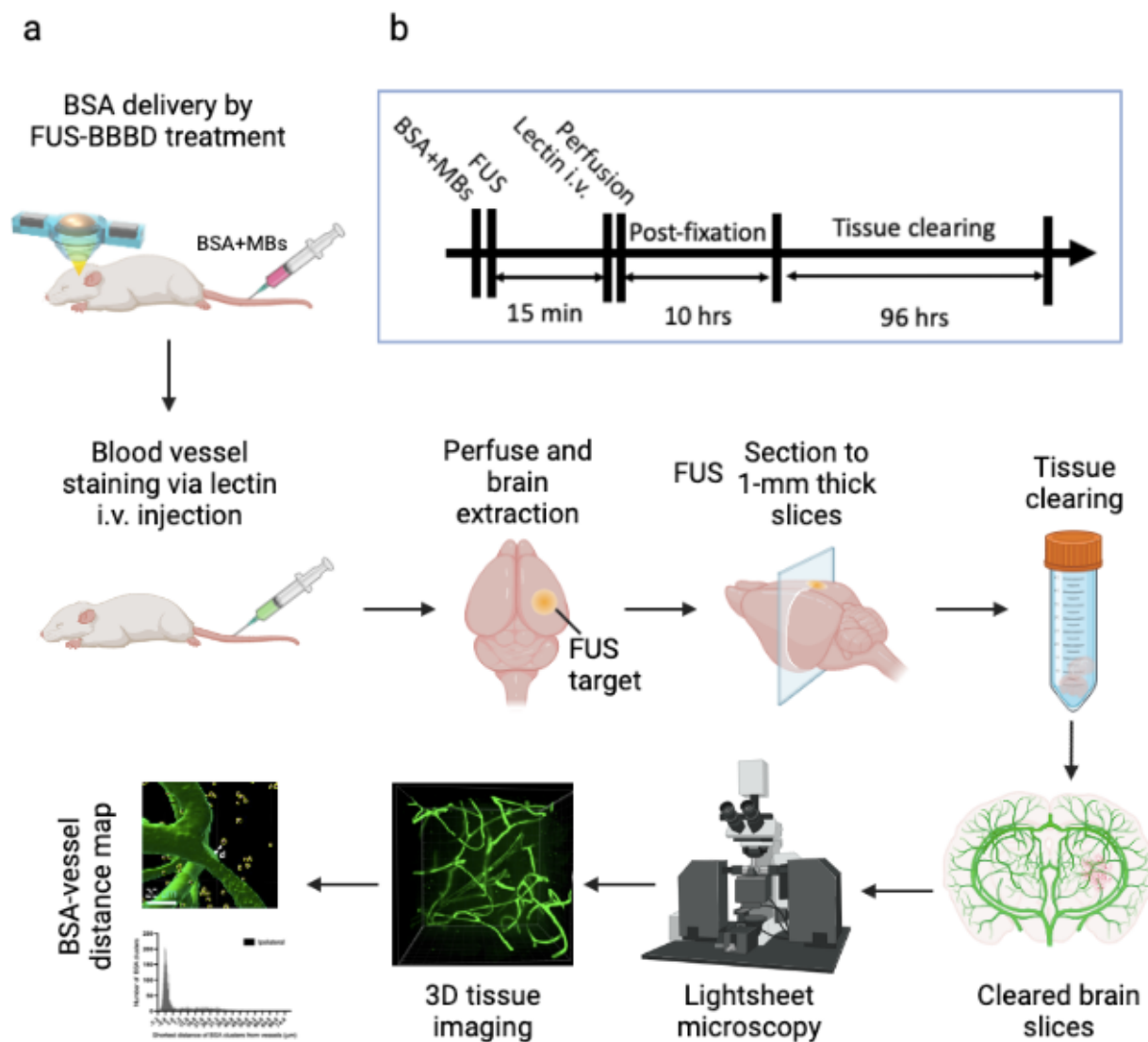Figure 2.1 Workflow and timeline.

(a) Workflow. (b) Timeline.

Experimental Procedure

BSA-AF647 Delivery via FUS-BBB Opening

6 mouses were anesthetized with a continuous flow of 2% isoflurane mixed with oxygen. Then BSA-AF647 (4.29 μg/kg) and microbubbles (5 x 10^8/kg) were injected into the mouse via tail vein. Treat the mouses with FUS setup on one side with different pressure (3 for 0.2

MPa and 3 for 0.4 MPa). The frequency of the FUS transducer is 1.5 MHz After 15 mins, inject Lycopersicon Esculentum (Tomato) Lectin conjugated with DyLight 488 (Thermo Fisher Scientific, Wilmington, DE, USA) into the mouse via tail vein, followed by perfusion immediately.

Transcardial Perfusion Fixation and Post-fixation

The transcardial perfusion was completed by a perfusion pump with a speed of 5.5 mL/min. First, the blood was removed by 60 mL perfusion solution containing 1x PBS, 10 U/mL heparin and 0.5% w/v sodium nitrite (Sigma Aldrich, St. Louis, MO, USA). Then the tissue was fixed by perfusion with 50 mL fixation solution containing 1x PBS and 4% w/v paraformaldehyde (PFA) (Sigma Aldrich, St. Louis, MO, USA). After being harvested from the mouse, the mouse brain was incubated in 4% PFA/PBS at 4 °C for 10 hours.

AbScale Clearing

The fixed brains were sectioned as 1 mm thick slices. Before clearing, samples were imaged by Pearl Trilogy Small Animal Imager to record the BSA delivery results. 2 slices with a strong signal were selected to be cleared for each mouse.

In this protocol, ScaleS0 solution is made by mixing 1x PBS, 20% w/v D-sorbitol (Sigma Aldrich, St. Louis, MO, USA), 1 mM Methyl-β-cyclodextrin (Sigma Aldrich, St. Louis, MO, USA), 1 mM γ-cyclodextrin (TCI Chemicals, Tokyo, Japan), N-acetyl-L-hydroxyproline (Oakwood Chemical, West Columbia, SC, USA), and 3% v/v Dimethyl sulfoxide (DMSO) and adjusting the pH to 7.2 with NaOH and HCl. ScaleA2 solution contains dd water, 10% w/v glycerol, 4 M urea and 0.1% Triton X-100. ScaleB4 solution is 8 M aqueous urea in dd water. ScaleS4 solution contains dd water, 40% w/v D-sorbitol, 10% w/v glycerol, 4 M urea, 15% DMSO and 0.1% Triton X-100.

Selected slices were first incubated in ScaleS0 solution for 12 hours to permeabilize the samples. Then the incubation solution was changed to ScaleA2 for 36 hours, followed by ScaleB4 for 24 hours and changed back to ScaleA2 for another 12 hours. All incubation was at 37 °C with shaking. The samples were washed with 1x PBS at 4 °C for 6 hours. Finally, the samples were moved to ScaleS4 solution and incubated at 37 °C for 12 hours before imaging (Figure 2.2).
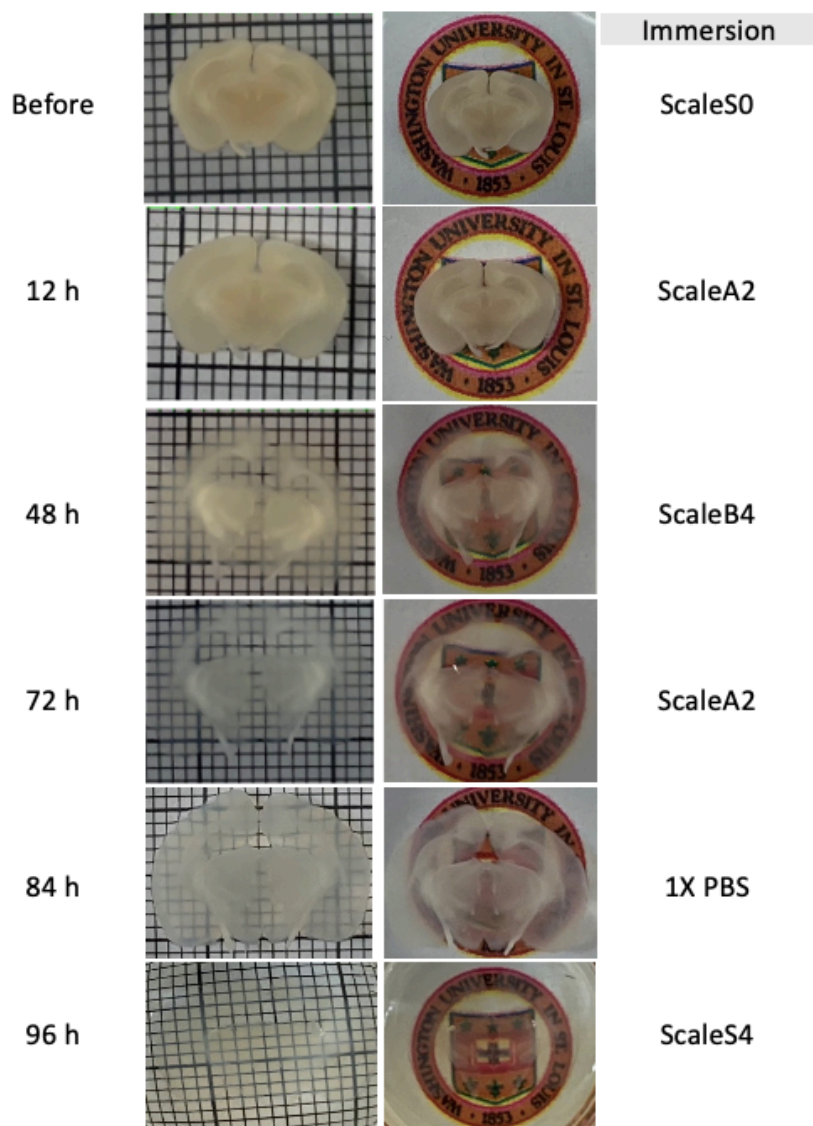
Figure 2.2 Tissue opacity throughout the clearing process.

Light-sheet Imaging

After tissue clearing, samples were imaged with Pearl Trilogy Small Animal Imager to record the BSA delivery results again. One pair of regions of interest (ROIs) was selected from the slice with a stronger signal for each brain to be imaged with the lightsheet microscopy. Each pair of ROIs contains one region on the ipsilateral side with the strongest signal and one symmetry region on the contralateral side.

3D imaging of clearing samples containing BSA-AF647 was done using the Zeiss Lightsheet 7 planar illumination microscope equipped with a 20X objective lens (NA=1, RI=1.46).

The selected sample for each brain was taped to a sample holder by Loctite Super Glue and incubated in the chamber full of ScaleS4 solution. The z step size was 0.57 um. The size of each ROI was $450 \times 450 \times \sim1500$ µm (x, y, z). Raw images were collected from the ROI on the ipsilateral sides followed by the ROI on the contralateral sides.

<center>Image Analysis</center>

BSA Cluster and Vessel Segmentation

Bitplane Imaris was used to analyze the raw images from lightsheet microscopy. Images were cropped to the size of 450 x 450 x 500 um. For each pair of images, the contralateral one was processed first. Surface, the built-in program in Imaris was used to segment vessels. According to the image of the lectin channel, vessels are segmented as intact as possible by adjusting the threshold. Then Spots function was used to detect BSA clusters. The threshold about mean intensity in the BSA channel was adjusted until there were no clusters in the space far from vessels. The assumption that BSA cannot transport cross BBB at all without FUS treatment was applied

here. Vessels on the ipsilateral side were segmented independently while BSA clusters were detected by the same threshold as the contralateral side processed previously.

Shortest Distance Map

The shortest distance (Figure 2.3) from BSA clusters to vessel was automatically calculated by Imaris. The data was exported as Excel files and imported into GraphPad Prism 9 for later analysis and statistical plotting.
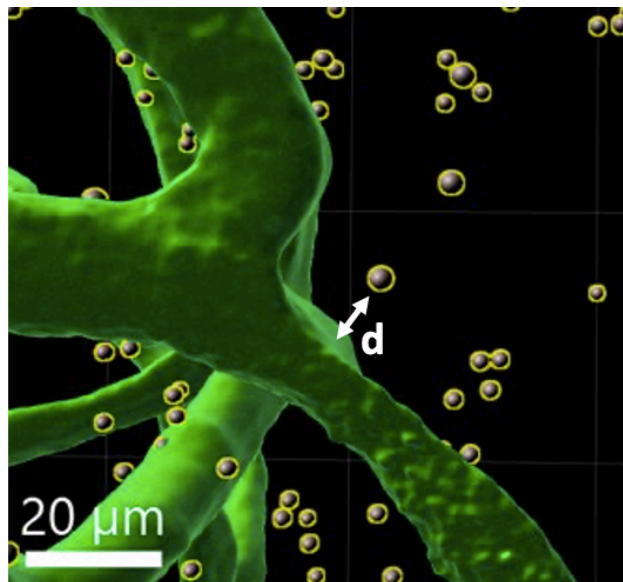

Figure 2.3 Definition of shortest distance from a BSA cluster to vessels.

Chapter 3: Results
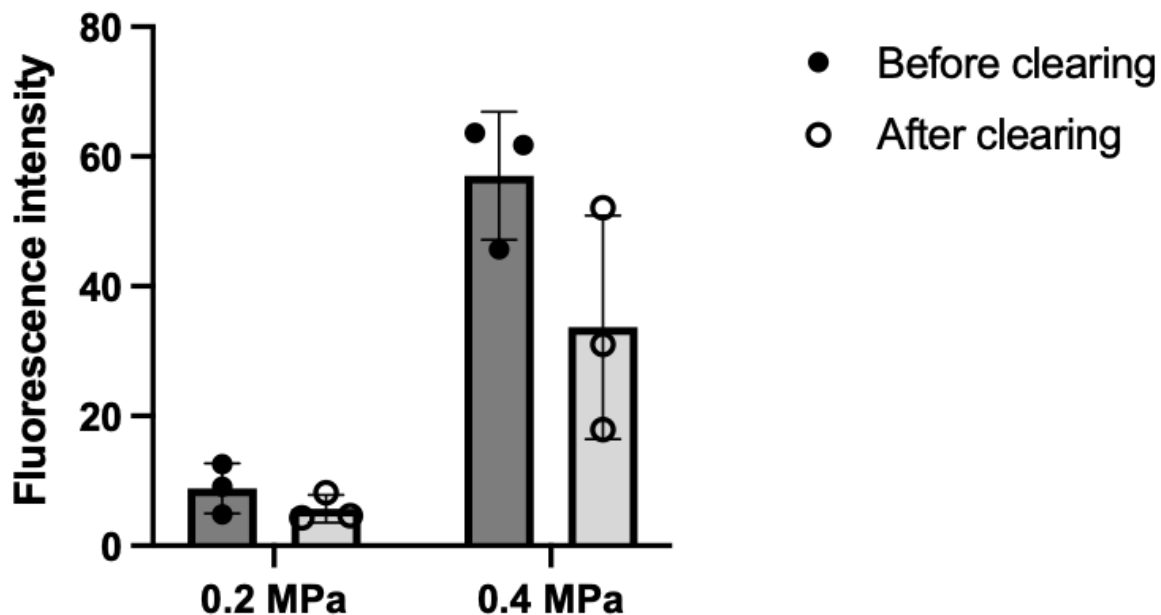
Effect of Tissue Clearing on FUS-delivered BSA

Figure 3.1 Fluorescence intensity in 2D images before and after tissue clearing, quantified by Pearl Trilogy Small Animal Imager and MATLAB code.

The mean fluorescence intensity of the BSA channel on samples treated 0.2 MPa FUS (Figure 3.1) has reduced 35.4% after clearing compared with before clearing. This ratio for 0.4 MPa samples is 41.0%.
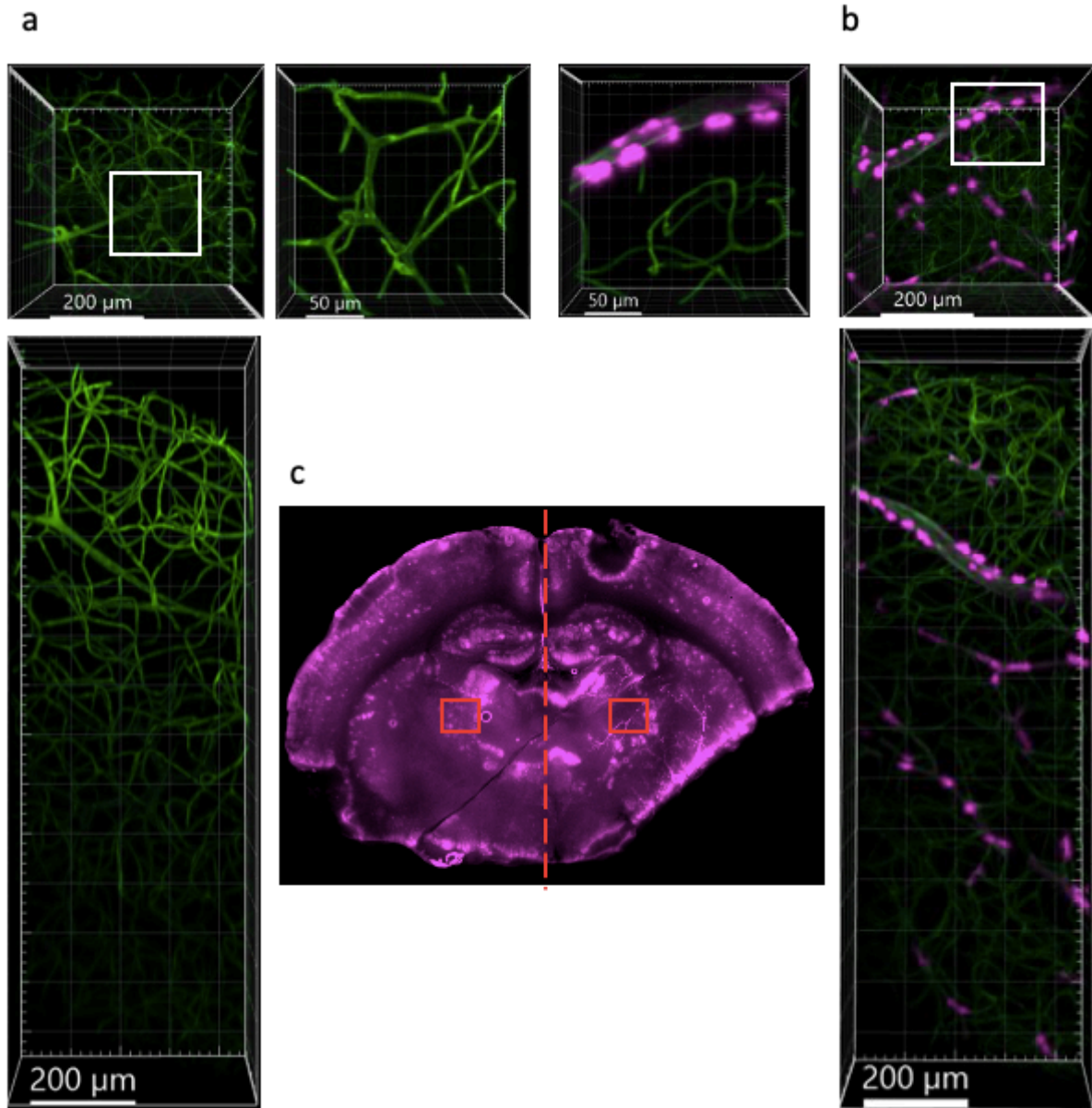
Quantification of BSA Clusters in 3D Images

Figure 3.2 Representative 3D images of lectin-stained blood vessels and BSA in cleared brain slices.

(a) Representative 3D images of the ROI on the contralateral side. The top figure is a top view and the bottom one is the side view. (b) BSA delivery result on the representative sample.

(c) Representative 3D images of the ROI on the ipsilateral side. Insets, 100 μm. The pressure of FUS used to treat this sample is 0.2 MPa.

Cleared mouse slices were imaged by an ORCA-Flash4.0 V3 Digital CMOS camera to show the BSA distribution on the whole slice (Figure 3.2 b). Each pair of ROI includes one area on the ipsilateral side which has apparent BSA retention and an area symmetrical to it. The red box in Figure 3.2b describes the approximate location of the ROI. With the lightsheet microscope, we obtained one pair of 3D images with a cross-section of 450×450 μm and a depth of approximately 1.5 mm from the ipsilateral side (Figure 3.2 c) and the contralateral side (Figure 3.2 a). The transparency of 1 mm-thick brain slices cleared with AbScale is enough for large volume 3D imaging. Under the same display setting, the BSA channel has apparently higher signal intensity on the ipsilateral side than the contralateral side. However, there is a lack of obvious difference of lectin between both sides. This indicates that BSA accumulated on the side treated with FUS within 15 minutes after the injection of BSA and the treatment of FUS. Since the size of the BSA single particle is much smaller than the resolution of the light sheet microscopy with 20× objective (lateral resolution: 1~2 μm), it is only able to distinguish clusters formed by BSA in these images.
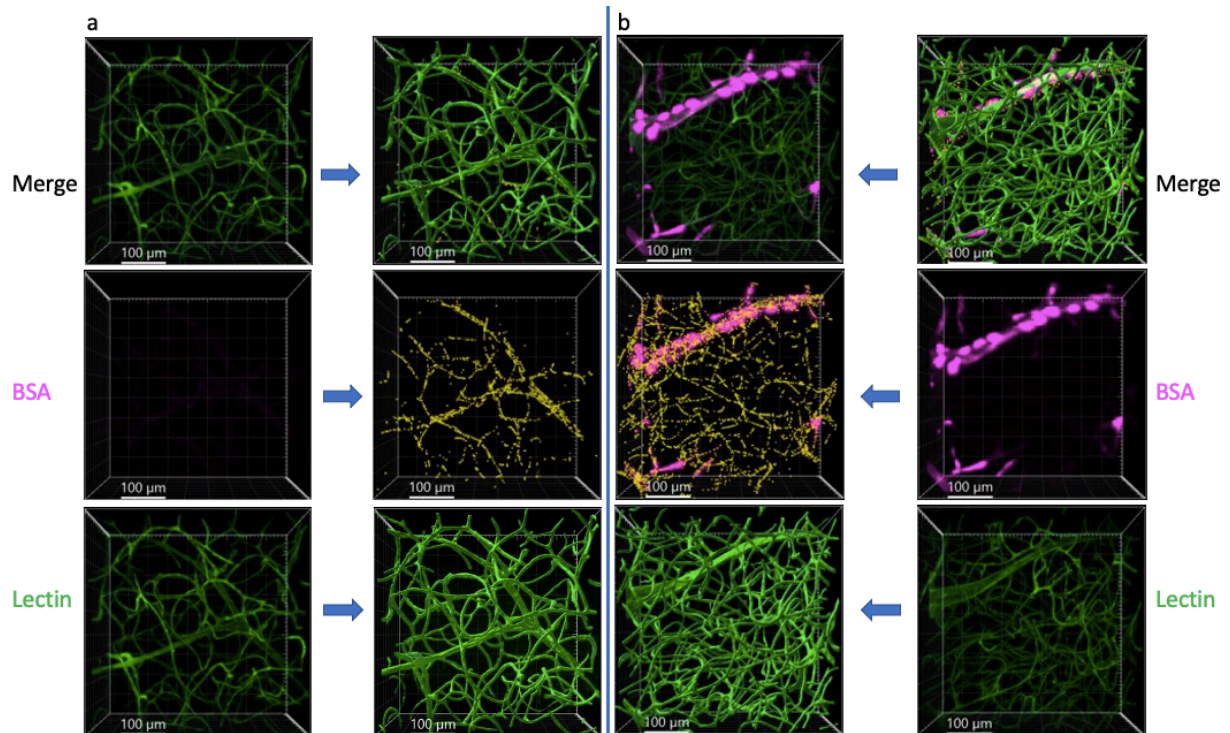
Figure 3.3 BSA cluster and blood vessel segmentation in representative 3D images.

(a) Raw images and processed images with BSA cluster and blood vessel segmentation from the contralateral side. Raw images are in the first column. Yellow spots in the second column represent segmented BSA clusters. Green surfaces represent segmented blood vessels. (b) Raw images and processed images with BSA cluster and blood vessel segmentation from the ipsilateral side. Raw images are in the second column. Size of all 3D images, 450 x 450 x 500 um. The pressure of FUS used to treat this sample is 0.2 MPa.

Compared to the raw image in Figure 3.3, the green surface is consistent with the distribution of blood vessels, showing that the vessel segmentation function can identify intact blood vessels stained with lectin and reflect their shape and spatial distribution. However, vessel segmentation faces difficulties in some areas where the fluorescence intensity is extremely low (the area indicated by the arrow in Figure 3.3a). Yellow spots are more

distributed on the ipsilateral side, which is consistent with what we observed in the raw image. Spots are denser where the fluorescence intensity of the BSA channel is stronger.
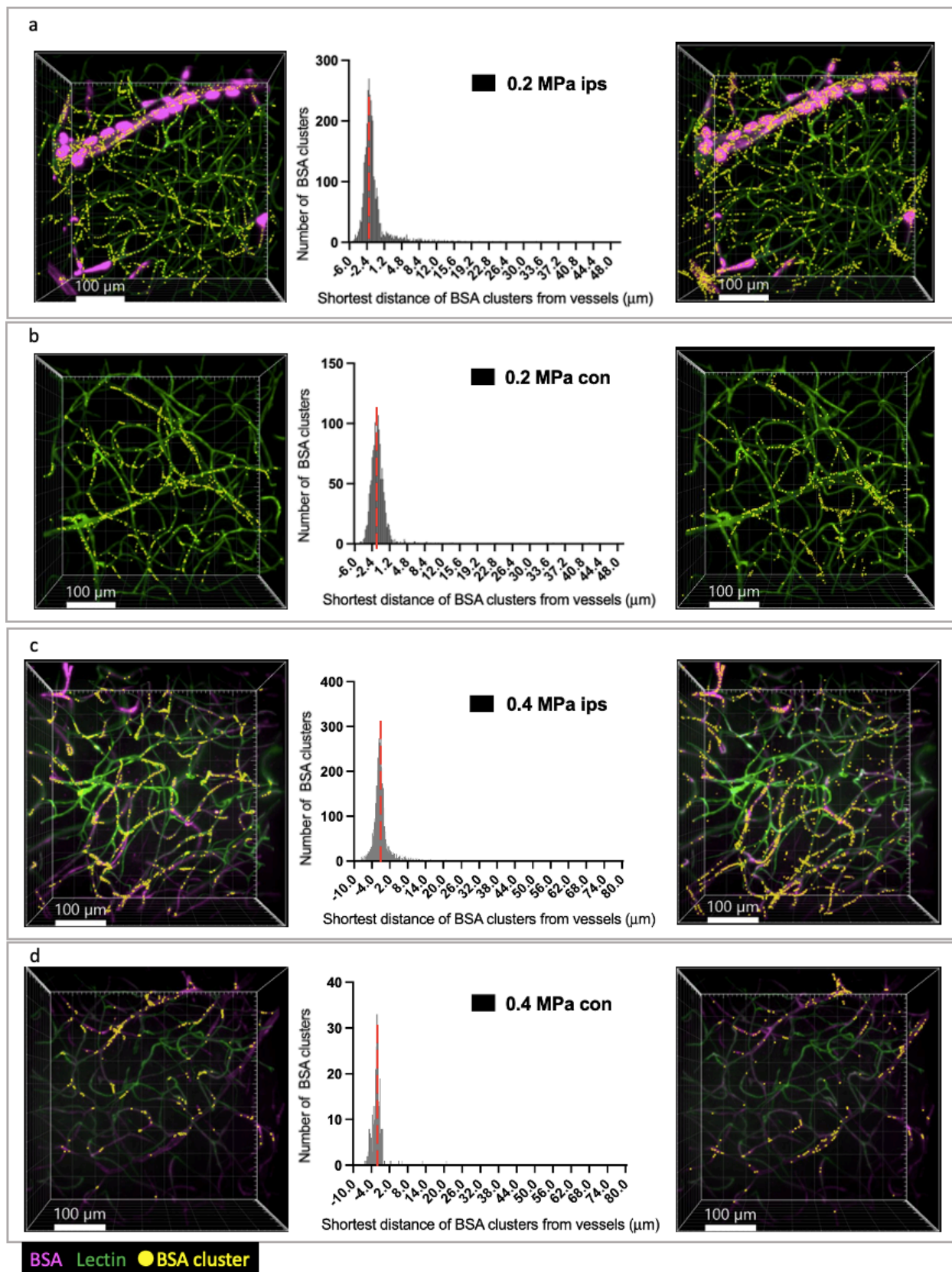
Figure 3.4 BSA cluster and blood vessel segmentation in representative 3D images.

(a) Raw images and processed images with BSA cluster and vessel segmentation from the contralateral side. Raw images are in the first column. Yellow spots in the second column represent segmented BSA clusters. Green surfaces represent segmented blood vessels. (b) Raw images and processed images with BSA cluster and blood vessel segmentation from the ipsilateral side. Raw images are in the second column. Size of all 3D images, 450 × 450 × 500 μm. The pressure of FUS used to treat this sample is 0.2 MPa.

Characterization of the BSA Delivery with the Distance Map

Peaks of all distance maps are located on the negative part of the x-axis, with a distance of around 1.5 μm to the zero points (Figure3.5). The differences in the peak locations among different conditions are insignificant. The location of the peak means where most BSA gathered. BSA uptake by vessels has been observed in untreated brains in the previous study.(Kucharz et al., 2021) It is acceptable to assume peaks in these distance maps are consistent with the location of vessels. However, lectin stains vessels on the luminal surface of ECs, (Robertson et al., 2015) so theoretically, peaks should locate on the positive part of the x-axis. Considering the resolution of lightsheet microscopy, this displacement can be explained by imaging artifacts.

Based on the previous assumption, clusters on the left of the peak represent a part of those taken up by vessels (Figure 3.4a iii). Since their locations are closer to the inner surface of vessels, we define them as inner part clusters. Clusters on the right of the peak of the distance map include a part of clusters located in vessels but closer to the outer surface of vessels, clusters adhered to the outer surface of vessels, and clusters delivered out of vessels (Figure 3.4b iii), which we define as outer part clusters.
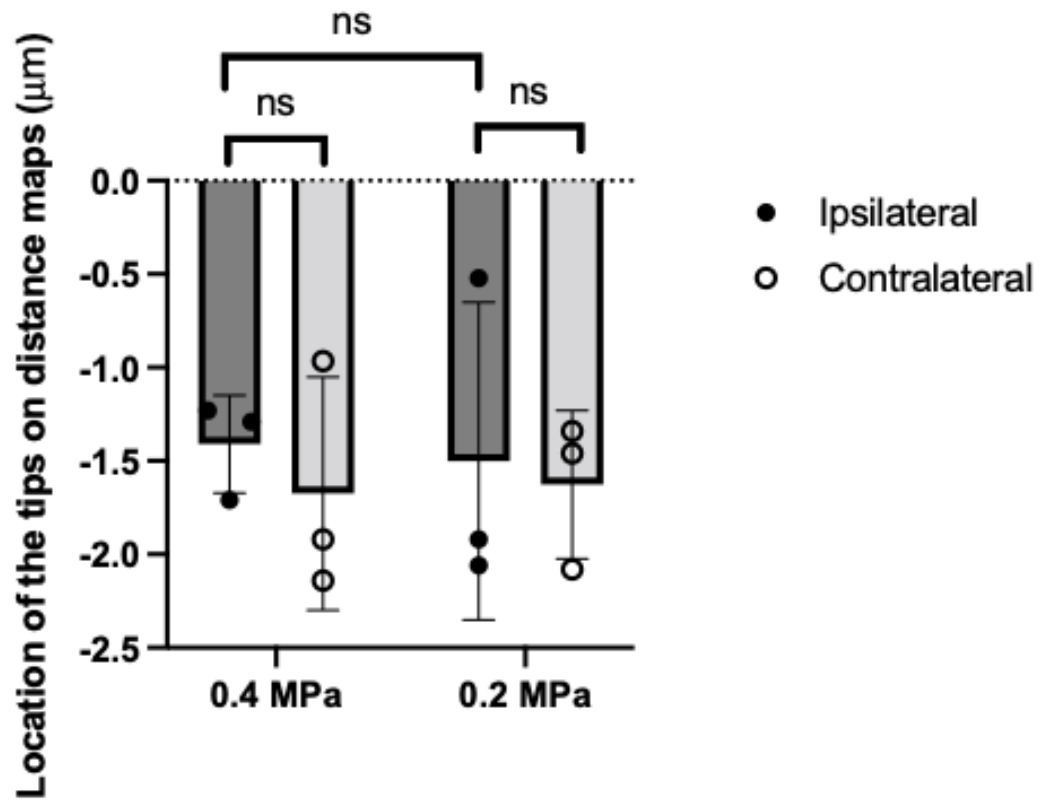
Figure 3.5 Locations of peaks on distance maps of BSA clusters delivered by FUS with the pressure of 0.4 MPa and 0.2 MPa on the ipsilateral and contralateral sides.
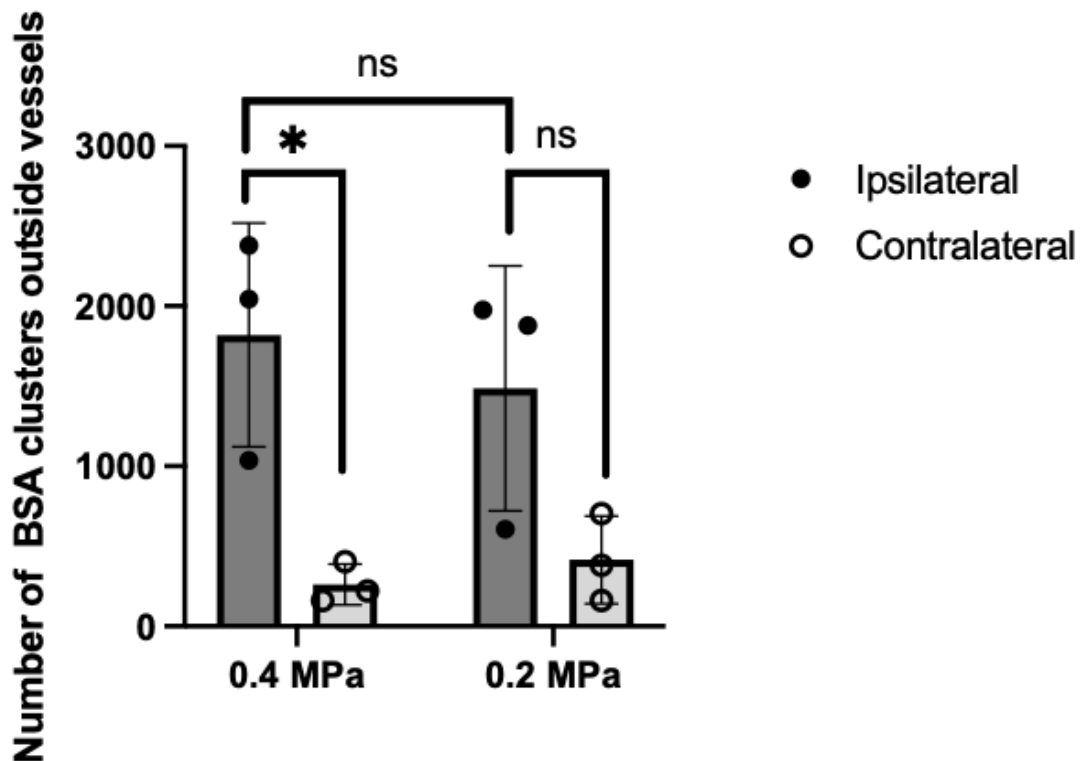
Figure 3.6 Quantification of outer part BSA clusters delivered by FUS with the pressure of 0.4 MPa and 0.2 MPa on the ipsilateral and contralateral sides. *P<0.05.

Figure 3.6 characterizes the BSA delivery level of different FUS pressure by the amount of BSA clusters on the right of the peak of the distance map. 0.4 MPa FUS has significant improvement on the outer part BSA delivery, increasing the mean number of clusters by 6.97-fold compared with the contralateral side. The fold for 0.2 MPa FUS is 3.58. However, there is no significant difference between 0.4 MPa and 0.2 MPa shown in this figure.
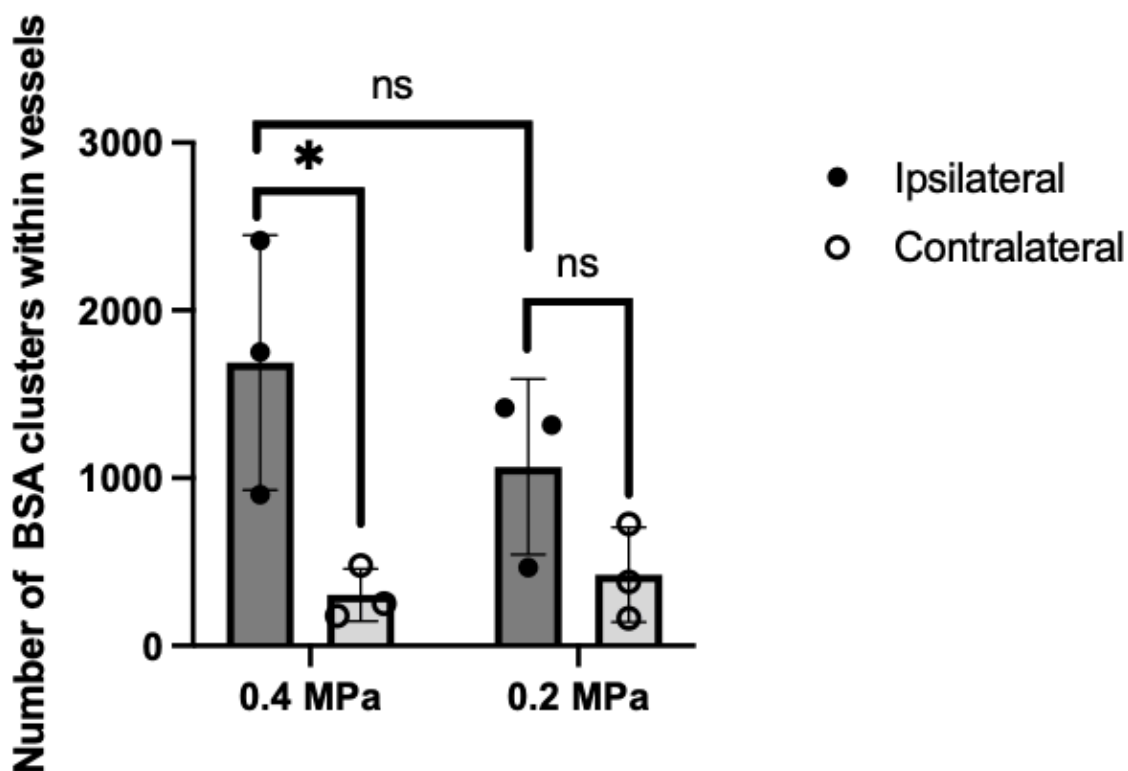
Figure 3.7 Quantification of inner part BSA clusters delivered by FUS with the pressure of 0.4 MPa and 0.2 MPa on the ipsilateral and contralateral sides. *P<0.05.

Figure 3.7 characterizes the BSA delivery level of different FUS pressure by the amount of BSA clusters on the left of the peak of the distance map. 0.4 MPa FUS has significant improvement on the inner part BSA, increasing the mean number of clusters by 5.58-fold compared with the contralateral side. The fold for 0.2 MPa FUS is 2.52. However, there is no significant difference in this characteristic between 0.4 MPa and 0.2 MPa.

Figure 3.8 The ratio of outer part BSA clusters to all clusters in the brain. *P<0.05.

Figure 3.8 characterizes the BSA delivery level of different FUS pressure by the ratio of BSA clusters on the right of the peak of the distance map to the total amount. 0.4 MPa FUS shows significant improvement on the outer part BSA delivery, increasing the mean ratio by 1.13-fold compared with the contralateral side. However, the fold for 0.2 MPa FUS is 1.10.
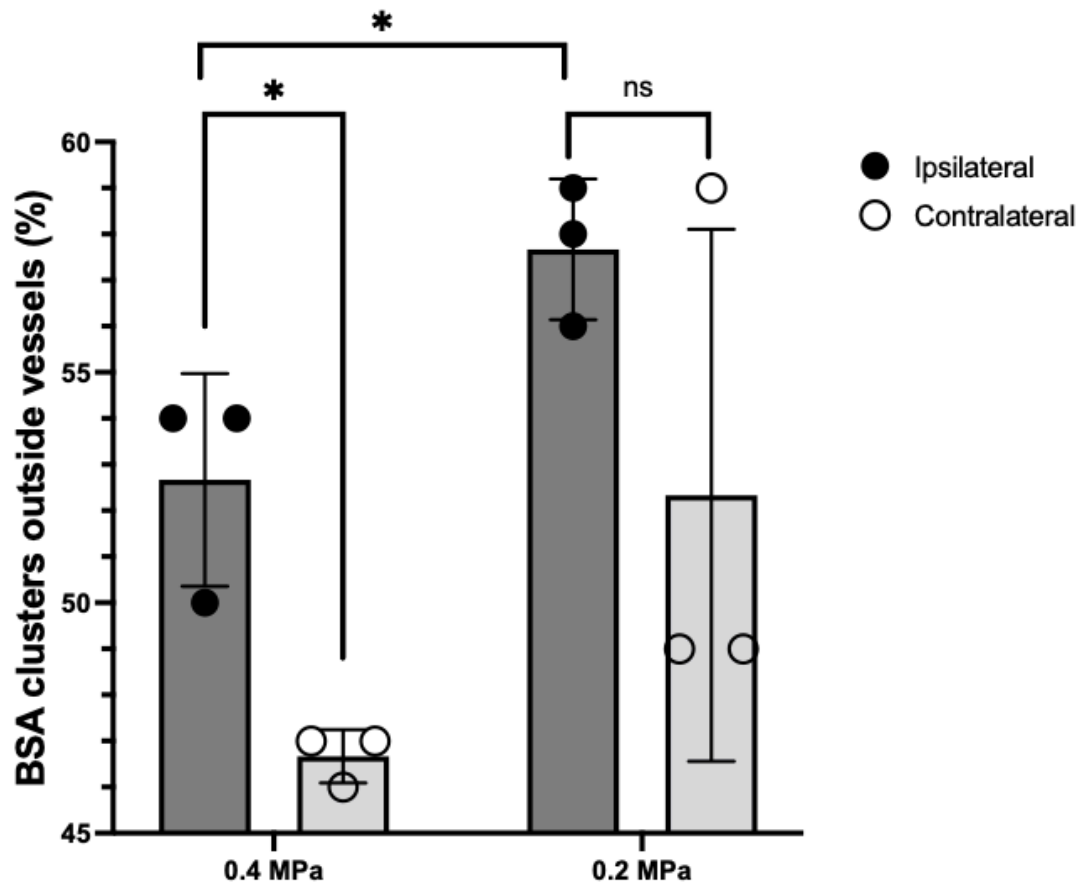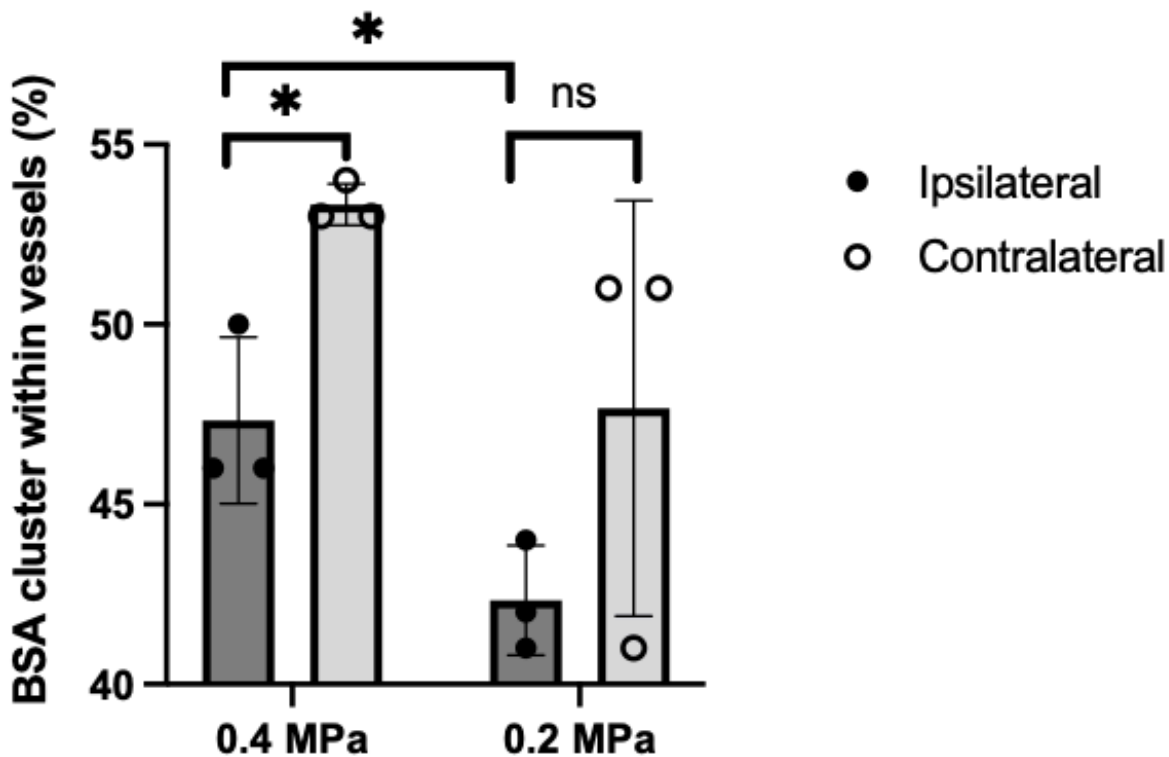
Figure 3.9 The ratio of inner part BSA clusters to all clusters in the brain. *P<0.05.

Figure 3.9 characterizes the BSA delivery level of different FUS pressure by the ratio of BSA clusters on the left of the peak of the distance map to the total amount. 0.4 MPa FUS significantly decrease the ratio of clusters by 18.7% compared with the contralateral side, which implies 0.4 MPa FUS has more improvement on outer part BSA delivery than the inner part. The decrease ratio for 0.2 MPa FUS is 11.2%.

Figure 3.10 Quantification of BSA clusters delivered to mouse brains by FUS with the pressure of 0.4 MPa and 0.2 MPa.

Figure 3.10 characterizes the BSA delivery level of different FUS pressure by the total amount of BSA clusters in the brain slice. 0.4 MPa FUS has significant improvement on the BSA delivery, increasing the mean number of clusters by 6.22-fold compared with the contralateral side. The fold for 0.2 MPa FUS is 3.19. However, it does not show a significant difference in this characteristic between 0.4 MPa and 0.2 MPa.
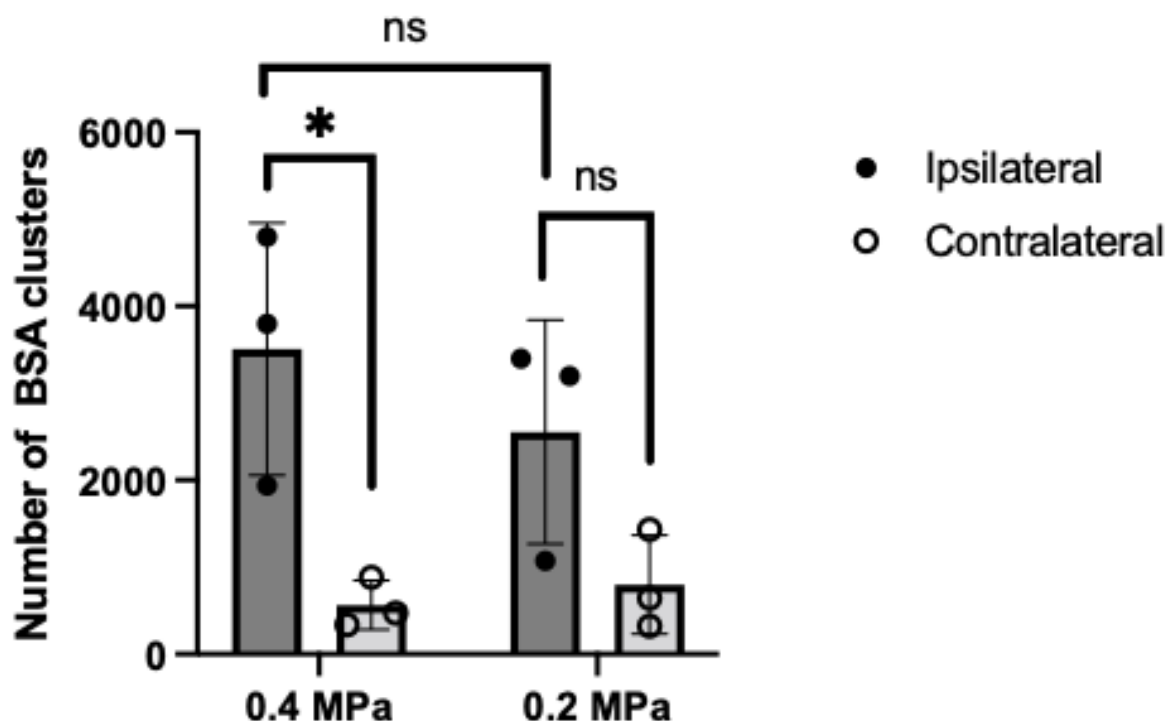
Although 0.2 MPa shows a significant difference compared with 0.4 MPa in Figure 3.9 and Figure 3.10, this difference may come from individual variation among samples rather than delivery capacity. The ratio of inner part clusters should be the same on the contralateral sides of 0.4 MPa samples and 0.2 MPa samples. However, in Figure 3.9 and Figure 3.10, there is an obvious difference between samples of two pressures. It is necessary to emphasize that the

threshold for BSA segmentation is only kept consistent between both sides on one sample, and the change of the threshold can influence the number and even ratio of inner and outer part clusters. In consequence, it does not make sense to compare the ipsilateral sides of 0.4 MPa and 0.2 MPa samples directly.

Chapter 4: Conclusion

Using the image analysis pipeline based on the shortest distance to analyze the 3D images of cleared brain slices following FUS treatment with different pressure, this study proved that 0.4 MPa FUS treatment can significantly enhance BSA delivery cross BBB, from both aspects of the inner part and outer part. whereas 0.2 MPa did not improve the delivery significantly. At the same time, this study also proved that this research pipeline has the potential to further study the spatial distribution of drugs delivered by FUS and the bioeffects of FUS treatment.

Chapter 5: Discussion

Limited by the resolution of light sheet microscopy, only BSA clusters are studied in this thesis. Single BSA particles diffused out of blood vessels can cause stronger background. However, it is difficult to quantify BSA single particles by the signal intensity of the background, since the background in images from light sheet microscopy is also influenced by the transparency of the ROI and the distance from the light source to the ROI.

BSA clusters far away from blood vessels mostly exist in the brain in the shape of ellipsoids. There is the possibility that those BSA were taken up by cells. In the future, immunostaining can be used to observe whether BSA clusters and some kinds of cells are co-localized to validate this assumption.

It's undeniable that this study has some direction that can be improved. Firstly, the number of replicates is not large enough, which might hide some information in the data. Secondly, although the wild filed microscope is used to select the ROI before 3D imaging, due to the different sizes of sample slices, it is difficult to accurately locate the ROI with the light sheet system after the sample is installed in the chamber. Establishing more rigorous installation procedures is expected to solve this problem. Besides, in the pilot study, 0.4 MPa FUS was used and BSA was allowed to cross the BBB for 1 hour. A more obvious contrast is observed on the ipsilateral side relative to the contralateral side. Reducing this time to 15 minutes has likely weakened the significance of the result. Last but not least, other experiments should be designed to quantify the reliability of the analysis pipeline.

References

Arms, L., Robson, A. L., Woldu, A., Martin, A., Palmer, W., Flynn, J., & Hua, S. (2020). Considerations for using optical clearing techniques for 3D imaging of nanoparticle biodistribution. *International Journal of Pharmaceutics*, *588*(June), 119739. https://doi.org/10.1016/j.ijpharm.2020.119739

Banks, W. A. (2008). The blood brain barrier. *Neuroimmune Pharmacology*, 21–38. https://doi.org/10.1007/978-0-387-72573-4_4

Chen, H., & Konofagou, E. E. (2014). The size of blood-brain barrier opening induced by focused ultrasound is dictated by the acoustic pressure. *Journal of Cerebral Blood Flow and Metabolism*, *34*(7), 1197–1204. https://doi.org/10.1038/jcbfm.2014.71

Chopra, R., Vykhodtseva, N., & Hynynen, K. (2010). Influence of exposure time and pressure amplitude on blood-brain-barrier opening using transcranial ultrasound exposures. *ACS Chemical Neuroscience*, *1*(5), 391–398. https://doi.org/10.1021/cn9000445

Cuccarese, M. F., Dubach, J. M., Pfirschke, C., Engblom, C., Garris, C., Miller, M. A., Pittet, M. J., & Weissleder, R. (2017). Heterogeneity of macrophage infiltration and therapeutic response in lung carcinoma revealed by 3D organ imaging. *Nature Communications*, *8*. https://doi.org/10.1038/ncomms14293

Dasgupta, A., Liu, M., Ojha, T., Storm, G., Kiessling, F., & Lammers, T. (2016). Ultrasound-mediated drug delivery to the brain: principles, progress and prospects. *Drug Discovery Today: Technologies*, *20*, 41–48. https://doi.org/10.1016/j.ddtec.2016.07.007

Dong, X. (2018). Current strategies for brain drug delivery. *Theranostics*, *8*(6), 1481–1493. https://doi.org/10.7150/thno.21254

Elzoghby, A. O., Samy, W. M., & Elgindy, N. A. (2012). Albumin-based nanoparticles as

potential controlled release drug delivery systems. *Journal of Controlled Release*, *157*(2), 168–182. https://doi.org/10.1016/j.jconrel.2011.07.031

Ertürk, A., Becker, K., Jährling, N., Mauch, C. P., Hojer, C. D., Egen, J. G., Hellal, F., Bradke, F., Sheng, M., & Dodt, H. U. (2012). Three-dimensional imaging of solvent-cleared organs using 3DISCO. *Nature Protocols*, *7*(11), 1983–1995. https://doi.org/10.1038/nprot.2012.119

Flynn, J., Martin, A., & Palmer, W. (2015). *3D tissue clearing with passive CLARITY: A handbook for HMRI/UoN researchers*. *October*, 1–24.

Gabathuler, R. (2010). Approaches to transport therapeutic drugs across the blood-brain barrier to treat brain diseases. *Neurobiology of Disease*, *37*(1), 48–57. https://doi.org/10.1016/j.nbd.2009.07.028

Galisteo-González, F., & Molina-Bolívar, J. A. (2014). Systematic study on the preparation of BSA nanoparticles. *Colloids and Surfaces B: Biointerfaces*, *123*, 286–292. https://doi.org/10.1016/j.colsurfb.2014.09.028

Hama, H., Hioki, H., Namiki, K., Hoshida, T., Kurokawa, H., Ishidate, F., Kaneko, T., Akagi, T., Saito, T., Saido, T., & Miyawaki, A. (2015). ScaleS: An optical clearing palette for biological imaging. *Nature Neuroscience*, *18*(10), 1518–1529. https://doi.org/10.1038/nn.4107

Hama, H., Kurokawa, H., Kawano, H., Ando, R., Shimogori, T., Noda, H., Fukami, K., Sakaue-Sawano, A., & Miyawaki, A. (2011). Scale: A chemical approach for fluorescence imaging and reconstruction of transparent mouse brain. *Nature Neuroscience*, *14*(11), 1481–1488. https://doi.org/10.1038/nn.2928

Ishizawa, K., Togami, K., Tada, H., & Chono, S. (2020). Evaluation of tissue-clearing

techniques for intraorgan imaging of distribution of polymeric nanoparticles as drug

carriers. *Drug Development and Industrial Pharmacy*, *46*(12), 2061–2069.

https://doi.org/10.1080/03639045.2020.1843476

Kucharz, K., Kristensen, K., Johnsen, K. B., Lund, M. A., Lønstrup, M., Moos, T., Andresen, T.

L., & Lauritzen, M. J. (2021). Post-capillary venules are the key locus for transcytosis-

mediated brain delivery of therapeutic nanoparticles. *Nature Communications*, *12*(1).

https://doi.org/10.1038/s41467-021-24323-1

Robertson, R. T., Levine, S. T., Haynes, S. M., Gutierrez, P., Baratta, J. L., Tan, Z., & Longmuir,

K. J. (2015). Use of labeled tomato lectin for imaging vasculature structures. *Histochemistry

and Cell Biology*, *143*(2), 225–234. https://doi.org/10.1007/s00418-014-1301-3

Sindhwani, S., Syed, A. M., Wilhelm, S., & Chan, W. C. W. (2017). Exploring passive clearing

for 3d optical imaging of nanoparticles in intact tissues. *Bioconjugate Chemistry*, *28*(1),

253–259. https://doi.org/10.1021/acs.bioconjchem.6b00500

Susaki, E. A., Tainaka, K., Perrin, D., Kishino, F., Tawara, T., Watanabe, T. M., Yokoyama, C.,

Onoe, H., Eguchi, M., Yamaguchi, S., Abe, T., Kiyonari, H., Shimizu, Y., Miyawaki, A.,

Yokota, H., & Ueda, H. R. (2014). Whole-brain imaging with single-cell resolution using

chemical cocktails and computational analysis. *Cell*, *157*(3), 726–739.

https://doi.org/10.1016/j.cell.2014.03.042

Yang, L., Feuchtinger, A., Möller, W., Ding, Y., Kutschke, D., Möller, G., Schittny, J. C.,

Burgstaller, G., Hofmann, W., Stoeger, T., Razansky, D., Walch, A., & Schmid, O. (2019).

Three-Dimensional Quantitative Co-Mapping of Pulmonary Morphology and Nanoparticle

Distribution with Cellular Resolution in Nondissected Murine Lungs. *ACS Nano*, *13*(2),

1029–1041. https://doi.org/10.1021/acsnano.8b07524